ECCOMAS Congress 2016
VII European Congress on Computational Methods in Applied Sciences and Engineering
M. Papadrakakis, V. Papadopoulos, G. Stefanou, V. Plevris (eds.)
Crete Island, Greece, 5–10 June 2016

ANALYTICAL SOLUTION FOR DYNAMIC FRACTURE OF TWO COPLANAR LIMITED-PERMEABLE CRACKS IN MAGNETO-ELECTRO-ELASTIC MATERIAL

Pei-Wei Zhang[1]

[1]Jiangsu Key Laboratory of Engineering Mechanics (Southeast University), School of Civil Engineering, Southeast University, No.2, Sipailou Street, Nanjing, 210096, P.R. China.
e-mail: zhangpeiwei@seu.edu.cn

Keywords: analytical solution; magneto-electro-elastic material; coplanar cracks; dynamic fracture; generalized intensity factor.

Abstract. *Two coplanar limited-permeable rectangular cracks in magneto-electro-elastic material are modeled and solved using generalized Almansi's theorem. The mixed boundary value problem is formulated into three pairs of dual integral equations with the help of Fourier transform, in which the unknown functions are the jumps of displacements across the crack-surface. By directly expanding the unknown functions into infinite series form of Jacobi polynomials, the dual integral equations are solved, and the analytical expressions of generalized intensity factors are derived strictly. Based on the generalized intensity factors, the dynamic behaviors of two cracks are estimated under P-wave loads. To show the trends of effects of loading frequency and geometry of cracks on the generalized intensity factors, top finite terms of infinite series are numerically calculated based on the Schmidt method. Numerical results are then drawn graphically. It reveals that the trend of two cracks forming a larger crack by propagating depends strongly on crack geometry and load frequency. This work illuminate the condition inducing different crack propagation patterns, which will benifit the forecast of damage forms of transversely isotropic magneto-electro-elastic material.*

1 INTRODUCTIO

Magneto-electro-elastic composites, with its root in the early work of Vansuchtelen[1], have been widely applied in science and engineering. Layered magneto-electro-elastic composites, as a basic form of various electromagnetic structures, usually manufactured using tape-casting technique and bonding method, achieve a historic high electromagnetic factor. The dynamic mechanical, magnetic and electric loads are inevitable in its service, which make the layered magnetic-electric-elastic components pregnant coplanar cracks or parallel cracks from the interface or other weak position. Furthermore, the initiation of cracks will result in the reduction of electromagnetic conversion efficiency, if not fail prematurely. Therefore, researching on the dynamic fracture behaviors of magneto-electro-elastic composites is very worthwhile[2, 3]. To obtain the reliable service life time and the reliable action of related devices and to prevent failure during service, most of works concerned about the dynamic fracture problems with assumption of transversely isotropic property. Among them, Zhong et al[4, 5] investigated the anti-plane and in-plane dynamic fracture problem, and the influence of various factors on the crack propagation orientation were discussed. Feng et al[6, 7] also made lots of effort on the dynamic fracture of magneto-electro-elastic medium. They discussed four kinds of ideal crack-face assumption, and based on energy release rate, the effect of crack-face assumption on the crack extension was unfolded. As discussed in previous work[7], the boundary condition on the crack surface was complex in piezoelectric/piezomagnetic composites. The limited-permeable boundary condition first proposed in Hao's work[8] for piezoelectric materials was developed into magneto-electro-elastic composites by Zhong et al[5] and Zhou et al[9], respectively.

Although there are a lot of works focusing on the anti-plane and in-plane problems, it is insufficient to analyzing the fracture behavior in 3-Dimensions. And, it is important to take multi-cracked 3D medium into account. Layered composites were prone to generating multiple cracks in the same layer due to periodical fatigue loads or manufacturing process, so investigating the interaction between coplanar cracks is necessary. During analyzing 3D crack, model of penny, elliptical and rectangular were the most commonly used types, in which rectangular crack model is over safety in the engineering analysis.

With the lack of 3D dynamic analysis of multi-cracked magneto-electro-elastic materials in mind, in this paper, the model of transversely isotropic magneto-electro-elastic materials are established with two coplanar rectangular cracks parallel to the isotropic plane. Here the steady-state effects of the loading frequency on the limited-permeable crack initiating behavior were investigated on. The double-cracked magneto-electro-elastic material problems were formulated to three pairs of dual integral equations through Fourier transform. By solving the dual integral equations with the jumps of displacements as unknown variables, the analytical generalized intensity factors were derived strictly in the forms of infinite series which comes from Jacobi polynomial expansion of the jumps of displacements. In order to reveal some implicit links between mixed boundary conditions and generalized intensity factors, numerical results of generalized intensity factors were depicted and some useful conclusions and laws were explained, including the possibility of two crack converging and the effects of the geometry of cracks and the load frequency on the crack extension. This contribution is available for further analyzing multi-cracked 3D magneto-electro-elastic materials.

2 MODELING AND BASIC EQUATIONS

The simplified model of transversely isotropic homogeneous magneto-electro-elastic material is adopted in the present problem. Consider two coplanar rectangular cracks inside the isotropic plane as shown in Fig. 1. These two cracks are situated at the region of $l_1 \le |x| \le l_3$ and $|y| \le l_2$ in the plane of $z = 0$ in Cartesian coordinate system (x, y, z). A uniform distributed normal harmonic load $\sigma_{zz}(x, y, 0) = -\sigma_0 e^{i\omega\tau}$ (here σ_0 and ω are the amplitude and the circular frequency of the incident load wave, respectively.) is directly applied on the upper and the lower crack-surfaces, to which the solution combining with a uniform field can be transformed into the solution to the double-cracked material with a remotely harmonic load according to the standard superposition technique in the fracture mechanics point of view.

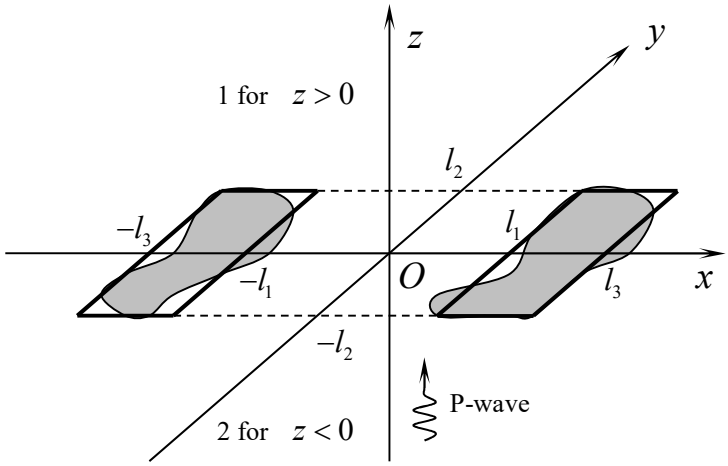

Fig.1: Geometry and coordinate system for two rectangular cracks

When the time-harmonic P-wave is applied on the magneto-electro-elastic materials and the response goes from the transient response stage into the steady state, all fields quantities can be expressed in the form as follows:

$$X_0(x, y, z, \tau) = X(x, y, z)e^{-i\omega\tau}$$

where X is on behalf of the displacement u_k , the electric potential ϕ , the magnetic potential ψ , the stress σ_{kl} , the electric displacements D_k and the magnetic flux B_k ($k, l = x, y, z$); τ is the time variable, respectively.

In Cartesian coordinates (x, y, z) of the present problem, the basic equations of linear, homogeneous, transversely isotropic magneto-electro-elastic material ignoring body force, free electric and magnetic charge are as follows:

$$\begin{cases} \sigma^{(j)}_{kl,k} = \rho_0 \ddot{u}^{(j)}_l \\ D^{(j)}_{k,k} = 0 \\ B^{(j)}_{k,k} = 0 \end{cases}, \qquad k, l = x, y, z \tag{1}$$

$$\begin{Bmatrix}\sigma_{xx}^{(j)}\\ \sigma_{yy}^{(j)}\\ \sigma_{zz}^{(j)}\\ \sigma_{xy}^{(j)}\\ \sigma_{xz}^{(j)}\\ \sigma_{yz}^{(j)}\end{Bmatrix}=\begin{bmatrix} c_{11}\partial_{,x} & c_{12}\partial_{,y} & c_{13}\partial_{,z} & e_{31}\partial_{,z} & q_{31}\partial_{,z}\\ c_{12}\partial_{,x} & c_{11}\partial_{,y} & c_{13}\partial_{,z} & e_{31}\partial_{,z} & q_{31}\partial_{,z}\\ c_{13}\partial_{,x} & c_{13}\partial_{,y} & c_{33}\partial_{,z} & e_{33}\partial_{,z} & q_{33}\partial_{,z}\\ (c_{11}-c_{12})\partial_{,y}/2 & (c_{11}-c_{12})\partial_{,x}/2 & 0 & 0 & 0\\ c_{44}\partial_{,z} & 0 & c_{44}\partial_{,x} & e_{15}\partial_{,x} & q_{15}\partial_{,x}\\ 0 & c_{44}\partial_{,z} & c_{44}\partial_{,y} & e_{15}\partial_{,y} & q_{15}\partial_{,y}\end{bmatrix}\begin{Bmatrix}u_x^{(j)}\\ u_y^{(j)}\\ u_z^{(j)}\\ \phi^{(j)}\\ \psi^{(j)}\end{Bmatrix} \tag{2}$$

$$\begin{Bmatrix}D_x^{(j)}\\ D_y^{(j)}\\ D_z^{(j)}\end{Bmatrix}=\begin{bmatrix} e_{15}\partial_{,z} & 0 & e_{15}\partial_{,x} & -\varepsilon_{11}\partial_{,x} & -d_{11}\partial_{,x}\\ 0 & e_{15}\partial_{,z} & e_{15}\partial_{,y} & -\varepsilon_{11}\partial_{,y} & -d_{11}\partial_{,y}\\ e_{31}\partial_{,x} & e_{31}\partial_{,y} & e_{33}\partial_{,z} & -\varepsilon_{33}\partial_{,z} & -d_{33}\partial_{,z}\end{bmatrix}\begin{Bmatrix}u_x^{(j)} & u_y^{(j)} & u_z^{(j)} & \phi^{(j)} & \psi^{(j)}\end{Bmatrix}^T \tag{3}$$

$$\begin{Bmatrix}B_x^{(j)}\\ B_y^{(j)}\\ B_z^{(j)}\end{Bmatrix}=\begin{bmatrix} q_{15}\partial_{,z} & 0 & q_{15}\partial_{,x} & -d_{11}\partial_{,x} & -\mu_{11}\partial_{,x}\\ 0 & q_{15}\partial_{,z} & q_{15}\partial_{,y} & -d_{11}\partial_{,y} & -\mu_{11}\partial_{,y}\\ q_{31}\partial_{,x} & q_{31}\partial_{,y} & q_{33}\partial_{,z} & -d_{33}\partial_{,z} & -\mu_{33}\partial_{,z}\end{bmatrix}\begin{Bmatrix}u_x^{(j)} & u_y^{(j)} & u_z^{(j)} & \phi^{(j)} & \psi^{(j)}\end{Bmatrix}^T \tag{4}$$

where ρ_0, c_{jk}, e_{jk}, ε_{jk}, q_{jk}, d_{jk} and μ_{jk} ($j,k=1,2,3$) are the mass density, the elastic stiffness constants, the piezoelectric constants, the electric permittivities, the piezomagnetic constants, the electromagnetic constants and the magnetic permeabilities of magneto-electro-elastic medium, respectively. $\ddot{u}_l^{(j)}$ denotes the second-order differential of $u_l^{(j)}$ with respect to time variable and a subscript comma denotes the partial differential to the coordinates (x,y,z), where the superscript j (j=1, 2) denotes the fields in the upper half space 1 ($z>0$) and the lower half space 2 ($z<0$) as shown in Fig.1. Considering the load wave propagating along z-axis in form of plane wave, $\ddot{u}_x^{(j)}=\ddot{u}_y^{(j)}=0$ is concluded.

Substituting Eqs.(2)-(4) into Eq.(1), the governing equations represented by the displacements, electric potentials and magnetic potentials are constructed:

$$\begin{cases}
c_{11}u_{x,xx}^{(j)}+(c_{11}-c_{12})u_{x,yy}^{(j)}/2+c_{44}u_{x,zz}^{(j)}+(c_{11}+c_{12})u_{y,xy}^{(j)}/2\\
\qquad +(c_{13}+c_{44})u_{z,xz}^{(j)}+(e_{15}+e_{31})\phi_{,xz}^{(j)}+(q_{15}+q_{31})\psi_{,xz}^{(j)}=0\\
(c_{11}-c_{12})u_{y,xx}^{(j)}/2+c_{11}u_{y,yy}^{(j)}+c_{44}u_{y,zz}^{(j)}+(c_{11}+c_{12})u_{x,xy}^{(j)}/2\\
\qquad +(c_{13}+c_{44})u_{z,yz}^{(j)}+(e_{15}+e_{31})\phi_{,yz}^{(j)}+(q_{15}+q_{31})\psi_{,yz}^{(j)}=0\\
c_{44}(u_{z,xx}^{(j)}+u_{z,yy}^{(j)})+c_{33}u_{z,zz}^{(j)}+(c_{13}+c_{44})(u_{x,xz}^{(j)}+u_{y,yz}^{(j)})\\
\qquad +e_{15}(\phi_{,xx}^{(j)}+\phi_{,yy}^{(j)})+e_{33}\phi_{,zz}^{(j)}+q_{15}(\psi_{,xx}^{(j)}+\psi_{,yy}^{(j)})+q_{33}\psi_{,zz}^{(j)}=-\omega^2\rho_0 u_z^{(j)}\\
e_{15}(u_{z,xx}^{(j)}+u_{z,yy}^{(j)})+e_{33}u_{z,zz}^{(j)}+(e_{15}+e_{31})(u_{x,xz}^{(j)}+u_{y,yz}^{(j)})\\
\qquad -\varepsilon_{11}(\phi_{,xx}^{(j)}+\phi_{,yy}^{(j)})-\varepsilon_{33}\phi_{,zz}^{(j)}-d_{11}(\psi_{,xx}^{(j)}+\psi_{,yy}^{(j)})-d_{33}\psi_{,zz}^{(j)}=0\\
q_{15}(u_{z,xx}^{(j)}+u_{z,yy}^{(j)})+q_{33}u_{z,zz}^{(j)}+(q_{15}+q_{31})(u_{x,xz}^{(j)}+u_{y,yz}^{(j)})\\
\qquad -d_{11}(\phi_{,xx}^{(j)}+\phi_{,yy}^{(j)})-d_{33}\phi_{,zz}^{(j)}-\mu_{11}(\psi_{,xx}^{(j)}+\psi_{,yy}^{(j)})-\mu_{33}\psi_{,zz}^{(j)}=0
\end{cases} \tag{5}$$

In magneto-electro-elastic material, the velocity of elastic P-wave in z -axis direction $c_z = \sqrt{(c_{33} + e_{33}\frac{e_{33}\mu_{33} - q_{33}d_{33}}{\varepsilon_{33}\mu_{33} - d_{33}^2} + q_{33}\frac{q_{33}\varepsilon_{33} - e_{33}d_{33}}{\mu_{33}\varepsilon_{33} - d_{33}^2}) / \rho_0}$ can be derived which only depends on the material constants.

3 LIMITED-PERMEABLE BOUNDARY CONDITIONS

The limited-permeable crack model, developed in Zhong's [10] and Zhou's [9, 11] works, is adopted here. The boundary conditions on crack-surfaces and at infinity for 3D problem are expressed in detail as follows:

$$\begin{cases} \sigma_{zz}^{(1)}(x,y,0^+) = \sigma_{zz}^{(2)}(x,y,0^-) = -\sigma_0 \\ \sigma_{xz}^{(1)}(x,y,0^+) = \sigma_{xz}^{(2)}(x,y,0^-) = 0, \quad \sigma_{yz}^{(1)}(x,y,0^+) = \sigma_{yz}^{(2)}(x,y,0^-) = 0 \\ D_z^{(1)}(x,y,0^+) = D_z^{(2)}(x,y,0^-), \quad B_z^{(1)}(x,y,0^+) = B_z^{(2)}(x,y,0^-) \qquad \text{for } l_1 \le |x| \le l_3, \\ D_{z0}[u_z^{(1)}(x,y,0^+) - u_z^{(2)}(x,y,0^-)] = \varepsilon_0[\phi^{(1)}(x,y,0^+) - \phi^{(2)}(x,y,0^-)] \\ B_{z0}[u_z^{(1)}(x,y,0^+) - u_z^{(2)}(x,y,0^-)] = \mu_0[\psi^{(1)}(x,y,0^+) - \psi^{(2)}(x,y,0^-)] \end{cases}$$

$$|y| \le l_2 \quad (6)$$

$$\begin{cases} \sigma_{zz}^{(1)}(x,y,0^+) = \sigma_{zz}^{(2)}(x,y,0^-), \quad \sigma_{xz}^{(1)}(x,y,0^+) = \sigma_{xz}^{(2)}(x,y,0^-) \\ \sigma_{yz}^{(1)}(x,y,0^+) = \sigma_{yz}^{(2)}(x,y,0^-), \quad u_x^{(1)}(x,y,0^+) = u_x^{(2)}(x,y,0^-) \\ u_y^{(1)}(x,y,0^+) = u_y^{(2)}(x,y,0^-), \quad u_z^{(1)}(x,y,0^+) = u_z^{(2)}(x,y,0^-) \qquad \text{for } |x| < l_1 \text{ or } |x| > l_3, \\ \phi^{(1)}(x,y,0^+) = \phi^{(2)}(x,y,0^-), \quad D_z^{(1)}(x,y,0^+) = D_z^{(2)}(x,y,0^-) \\ \psi^{(1)}(x,y,0^+) = \psi^{(2)}(x,y,0^-), \quad B_z^{(1)}(x,y,0^+) = B_z^{(2)}(x,y,0^-) \end{cases}$$

$$|y| > l_2 \quad (7)$$

$$u_x^{(j)}(x,y,z) = u_y^{(j)}(x,y,z) = u_z^{(j)}(x,y,z) = \phi^{(j)}(x,y,z) = \psi^{(j)}(x,y,z) = 0 \quad \text{for} \sqrt{x^2 + y^2 + z^2} \to \infty \quad (8)$$

where D_{z0} and B_{z0} are defined as the electric displacement and the magnetic flux inside cracks, and they are equal to $D_z^{(1)}(x,y,0^+)$ and $B_z^{(1)}(x,y,0^+)$ in magnitude, respectively. As discussed in public literatures[10, 12], the electric displacement and magnetic induction inside the opening crack are almost constants and dependent on applied magneto-electro-elastic loads, material properties, dielectric permittivity and magnetic permeability of crack interior, which would be certified briefly later. The limited-permeable boundary conditions in Eq.(6) will transform to permeable electric-magnetic boundary condition when $u_z^{(1)}(x,y,0^+) - u_z^{(2)}(x,y,0^-) = 0$ and to impermeable one when $\varepsilon_0 = \mu_0 = 0$.

4 SOLUTION PROCEDURE

The governing equations (5) need to be simplified by introducing displacement potential functions as discussed in reference [13]. Let

$$u_x^{(j)} = \Psi_{,y}^{(j)} - G_{,x}^{(j)}, \quad u_y^{(j)} = -\Psi_{,x}^{(j)} - G_{,y}^{(j)} \tag{9}$$

where $\Psi^{(j)}$ and $G^{(j)}$ are two potential functions. By strict derivation, the general expressions of the displacement potential function, the displacements, stresses, electric potentials, electric displacements, magnetic potentials and magnetic flux fields satisfying Eq. (8) are derived as follows:

$$\begin{cases} G^{(1)}(x,y,z) = \dfrac{4}{\pi^2}\int_0^\infty\int_0^\infty \sum_{k=1}^{4} \chi_k^{(1)}(s,t)A_k(s,t)\cos(sx)\cos(ty)e^{-\lambda_k\sqrt{s^2+t^2}z}dsdt \\ u_x^{(1)}(x,y,z) = \dfrac{4}{\pi^2}\int_0^\infty\int_0^\infty [tA_0(s,t)e^{-\lambda_0\sqrt{s^2+t^2}z} + s\sum_{k=1}^{4} \chi_k^{(1)}(s,t)A_k(s,t)e^{-\lambda_k\sqrt{s^2+t^2}z}]\sin(sx)\cos(ty)dsdt \\ u_y^{(1)}(x,y,z) = \dfrac{4}{\pi^2}\int_0^\infty\int_0^\infty [-sA_0(s,t)e^{-\lambda_0\sqrt{s^2+t^2}z} + t\sum_{k=1}^{4} \chi_k^{(1)}(s,t)A_k(s,t)e^{-\lambda_k\sqrt{s^2+t^2}z}]\cos(sx)\sin(ty)dsdt \\ u_z^{(1)}(x,y,z) = \dfrac{4}{\pi^2}\int_0^\infty\int_0^\infty \sum_{k=1}^{4} \chi_k^{(2)}(s,t)A_k(s,t)\cos(sx)\cos(ty)e^{-\lambda_k\sqrt{s^2+t^2}z}dsdt \\ \phi^{(1)}(x,y,z) = \dfrac{4}{\pi^2}\int_0^\infty\int_0^\infty \sum_{k=1}^{4} \chi_k^{(3)}(s,t)A_k(s,t)\cos(sx)\cos(ty)e^{-\lambda_k\sqrt{s^2+t^2}z}dsdt \\ \psi^{(1)}(x,y,z) = \dfrac{4}{\pi^2}\int_0^\infty\int_0^\infty \sum_{k=1}^{4} \chi_k^{(4)}(s,t)A_k(s,t)\cos(sx)\cos(ty)e^{-\lambda_k\sqrt{s^2+t^2}z}dsdt \end{cases} \tag{10}$$

$$\begin{cases} G^{(2)}(x,y,z) = \dfrac{4}{\pi^2}\int_0^\infty\int_0^\infty \sum_{k=1}^{4} \chi_k^{(1^*)}(s,t)B_k(s,t)\cos(sx)\cos(ty)e^{\lambda_k\sqrt{s^2+t^2}z}dsdt \\ u_x^{(2)}(x,y,z) = \dfrac{4}{\pi^2}\int_0^\infty\int_0^\infty [tB_0(s,t)e^{\lambda_0\sqrt{s^2+t^2}z} + s\sum_{k=1}^{4} \chi_k^{(1^*)}(s,t)B_k(s,t)e^{\lambda_k\sqrt{s^2+t^2}z}]\sin(sx)\cos(ty)dsdt \\ u_y^{(2)}(x,y,z) = \dfrac{4}{\pi^2}\int_0^\infty\int_0^\infty [-sB_0(s,t)e^{\lambda_0\sqrt{s^2+t^2}z} + t\sum_{k=1}^{4} \chi_k^{(1^*)}(s,t)B_k(s,t)e^{\lambda_k\sqrt{s^2+t^2}z}]\cos(sx)\sin(ty)dsdt \\ u_z^{(2)}(x,y,z) = \dfrac{4}{\pi^2}\int_0^\infty\int_0^\infty \sum_{k=1}^{4} \chi_k^{(2^*)}(s,t)B_k(s,t)\cos(sx)\cos(ty)e^{\lambda_k\sqrt{s^2+t^2}z}dsdt \\ \phi^{(2)}(x,y,z) = \dfrac{4}{\pi^2}\int_0^\infty\int_0^\infty \sum_{k=1}^{4} \chi_k^{(3^*)}(s,t)B_k(s,t)\cos(sx)\cos(ty)e^{\lambda_k\sqrt{s^2+t^2}z}dsdt \\ \psi^{(2)}(x,y,z) = \dfrac{4}{\pi^2}\int_0^\infty\int_0^\infty \sum_{k=1}^{4} \chi_k^{(4^*)}(s,t)B_k(s,t)\cos(sx)\cos(ty)e^{\lambda_k\sqrt{s^2+t^2}z}dsdt \end{cases} \tag{11}$$

where $\chi_k^{(j)}(s,t)$ and $\chi_k^{(j^*)}(s,t)$ ($k = 1,2,3,4.\quad j = 1,2,3,4,5.$) are functions of known expressions (The expressions are not shown here for brevity.).

$$\begin{cases} \sigma_{zz}^{(1)}(x,y,z)=\dfrac{4}{\pi^2}\int_0^\infty\int_0^\infty\sum_{k=1}^{4}\beta_k^{(1)}(s,t)A_k(s,t)e^{-\lambda_k\sqrt{s^2+t^2}z}\cos(sx)\cos(ty)dsdt \\ \sigma_{yz}^{(1)}(x,y,z)=\dfrac{4}{\pi^2}\int_0^\infty\int_0^\infty\sum_{k=1}^{5}\beta_k^{(2)}(s,t)A_k(s,t)e^{-\lambda_k\sqrt{s^2+t^2}z}\cos(sx)\sin(ty)dsdt \\ \sigma_{xz}^{(1)}(x,y,z)=\dfrac{4}{\pi^2}\int_0^\infty\int_0^\infty\sum_{k=1}^{5}\beta_k^{(3)}(s,t)A_k(s,t)e^{-\lambda_k\sqrt{s^2+t^2}z}\sin(sx)\cos(ty)dsdt \\ D_z^{(1)}(x,y,z)=\dfrac{4}{\pi^2}\int_0^\infty\int_0^\infty\sum_{k=1}^{4}\beta_k^{(4)}(s,t)A_k(s,t)e^{-\lambda_k\sqrt{s^2+t^2}z}\cos(sx)\cos(ty)dsdt \\ B_z^{(1)}(x,y,z)=\dfrac{4}{\pi^2}\int_0^\infty\int_0^\infty\sum_{k=1}^{4}\beta_k^{(5)}(s,t)A_k(s,t)e^{-\lambda_k\sqrt{s^2+t^2}z}\cos(sx)\cos(ty)dsdt \end{cases} \tag{12}$$

$$\begin{cases} \sigma_{zz}^{(2)}(x,y,z)=\dfrac{4}{\pi^2}\int_0^\infty\int_0^\infty\sum_{k=1}^{4}\beta_k^{(1*)}(s,t)B_k(s,t)\cos(sx)\cos(ty)e^{\lambda_k\sqrt{s^2+t^2}z}dsdt \\ \sigma_{yz}^{(2)}(x,y,z)=\dfrac{4}{\pi^2}\int_0^\infty\int_0^\infty\sum_{k=1}^{5}\beta_k^{(2*)}(s,t)B_k(s,t)\cos(sx)\sin(ty)e^{\lambda_k\sqrt{s^2+t^2}z}dsdt \\ \sigma_{xz}^{(2)}(x,y,z)=\dfrac{4}{\pi^2}\int_0^\infty\int_0^\infty\sum_{k=1}^{5}\beta_k^{(3*)}(s,t)B_k(s,t)\sin(sx)\cos(ty)e^{\lambda_k\sqrt{s^2+t^2}z}dsdt \\ D_z^{(2)}(x,y,z)=\dfrac{4}{\pi^2}\int_0^\infty\int_0^\infty\sum_{k=1}^{4}\beta_k^{(4*)}(s,t)B_k(s,t)\cos(sx)\cos(ty)e^{\lambda_k\sqrt{s^2+t^2}z}dsdt \\ B_z^{(2)}(x,y,z)=\dfrac{4}{\pi^2}\int_0^\infty\int_0^\infty\sum_{k=1}^{4}\beta_k^{(5*)}(s,t)B_k(s,t)\cos(sx)\cos(ty)e^{\lambda_k\sqrt{s^2+t^2}z}dsdt \end{cases} \tag{13}$$

where $\beta_k^{(j)}(s,t)$ and $\beta_k^{(j^*)}(s,t)$ ($k=0,1,2,3,4.\quad j=1,2,3,4,5.$) are functions of known expressions (The expressions are not shown here for brevity.).

Substitution of expressions (10)-(11) into limited-permeable boundary condition (6), electric displacement and magnetic flux inside crack can be generated

$$\begin{cases} D_{z0}=\varepsilon_0\dfrac{\sum_{k=1}^{4}\chi_k^{(3)}(s,t)[A_k(s,t)+B_k(s,t)]}{\sum_{k=1}^{4}\chi_k^{(2)}(s,t)[A_k(s,t)+B_k(s,t)]} \\ B_{z0}=\mu_0\dfrac{\sum_{k=1}^{4}\chi_k^{(4)}(s,t)[A_k(s,t)+B_k(s,t)]}{\sum_{k=1}^{4}\chi_k^{(2)}(s,t)[A_k(s,t)+B_k(s,t)]} \end{cases} \tag{14}$$

It is obviously that the distribution of electric displacement and magnetic flux inside crack is independent on Cartesian coordinates, means, both of the physical field inside cracks are almost constants.

To solve the fracture problem, the jumps of displacement on upper and lower crack surface are defined as follows:

$$\begin{cases} f_1(x,y) = u_x^{(1)}(x,y,0^+) - u_x^{(2)}(x,y,0^-) \\ f_2(x,y) = u_y^{(1)}(x,y,0^+) - u_y^{(2)}(x,y,0^-) \\ f_3(x,y) = u_z^{(1)}(x,y,0^+) - u_z^{(2)}(x,y,0^-) \end{cases} \tag{15}$$

It is obviously that both $f_1(x,y)$ and $f_3(x,y)$ are even functions about the variable y and $f_2(x,y)$ is an odd function about the variable y according to the symmetry of this problem.

Using Fourier transform, and Substituting Eqs.(10)-(13) into the crack boundary conditions Eqs.(6)-(7) and the jumps of displacements Eq.(15), the following dual integral equations can be deduced:

$$\sigma_{zz}^{(1)}(x,y,0) = \frac{2}{\pi^2}\int_0^\infty\int_0^\infty g_1(s,t)\overline{f}_3(s,t)\cos(sx)\cos(ty)dsdt = -\sigma_0, \qquad l_1 \le x \le l_3 \text{ and } 0 \le y \le l_2 \tag{16}$$

$$\sigma_{xz}^{(1)}(x,y,0) = \frac{2}{\pi^2}\int_0^\infty\int_0^\infty [g_2(s,t)\overline{f}_1(s,t) + g_3(s,t)\overline{f}_2(s,t)]\sin(sx)\cos(ty)dsdt = 0, \quad l_1 \le x \le l_3 \text{ and } 0 \le y \le l_2 \tag{17}$$

$$\sigma_{yz}^{(1)}(x,y,0) = \frac{2}{\pi^2}\int_0^\infty\int_0^\infty [g_4(s,t)\overline{f}_1(s,t) + g_5(s,t)\overline{f}_2(s,t)]\cos(sx)\sin(ty)dsdt = 0, \quad l_1 \le x \le l_3 \text{ and } 0 \le y \le l_2 \tag{18}$$

$$\begin{cases} \int_0^\infty\int_0^\infty \overline{f}_1(s,t)\sin(sx)\cos(ty)dsdt = 0 \\ \int_0^\infty\int_0^\infty \overline{f}_2(s,t)\cos(sx)\sin(ty)dsdt = 0, \quad \text{for } |x| < l_1 \text{ or } |x| > l_3 \text{ or } y > l_2 \\ \int_0^\infty\int_0^\infty \overline{f}_3(s,t)\cos(sx)\cos(ty)dsdt = 0 \end{cases} \tag{19}$$

where $\overline{f}_j(s,t)$ $(j=1,2,3)$ indicates two dimensional Fourier transform of $f_j(x,y)$. $g_k(s,t)$ $(k=1,2,3,4,5.)$ are known functions (The forms of functions are not shown here for brevity.). The foregoing three pairs of dual integral equations (16)-(19) must be solved to determine the unknown functions $f_1(x,y)$, $f_2(x,y)$ and $f_3(x,y)$.

5 CRACK TIP SINGULARITY FIELD AND GENERALIZED INTENSITY FACTOR

The Schmidt method [14-16] is introduced to solve the dual integral equations (16)-(19). The whole generalized fields can be solved, such as stress, electric displacement, magnetic flux and so on. But, to determine the generalized field intensity factors, the main attention must be focused on the generalized fields ahead of crack edges. In this work, $\sigma_{zz}^{(1)}$, $\sigma_{xz}^{(1)}$, $\sigma_{yz}^{(1)}$, $D_z^{(1)}$ and $B_z^{(1)}$ ahead of crack edges are obtained as follows:

$$\sigma_{zz}^{(1)}(x,y,0) = \frac{2}{\pi^2}\sum_{n=0}^{\infty}\sum_{m=0}^{\infty} c_{mn}\int_0^\infty \frac{1}{t}J_{2n+1}(tl_2)\cos(ty)dt\left[\int_0^\infty \frac{G_{mn}^{(3)}(s)}{s} g_1(s,t)J_{m+1}\left(s\frac{1-l_1}{2}\right)\cos(sx)ds\right] \tag{20}$$

$$\sigma_{xz}^{(1)}(x,y,0)=\sigma_{yz}^{(1)}(x,y,0)=0 \tag{21}$$

$$D_z^{(1)}(x,y,0)=\frac{2}{\pi^2}\sum_{n=0}^{\infty}\sum_{m=0}^{\infty}c_{mn}\int_0^{\infty}\frac{1}{t}J_{2n+1}(tl_2)\cos(ty)dt[\int_0^{\infty}\frac{G_{mn}^{(3)}(s)}{s}g_7(s,t)J_{m+1}(s\frac{1-l_1}{2})\cos(sx)ds] \tag{22}$$

$$B_z^{(1)}(x,y,0)=\frac{2}{\pi^2}\sum_{n=0}^{\infty}\sum_{m=0}^{\infty}c_{mn}\int_0^{\infty}\frac{1}{t}J_{2n+1}(tl_2)\cos(ty)dt[\int_0^{\infty}\frac{G_{mn}^{(3)}(s)}{s}g_8(s,t)J_{m+1}(s\frac{1-l_1}{2})\cos(sx)ds] \tag{23}$$

where $g_k(s,t)$ ($k=7,8$.) is known functions (The forms of functions are not shown here for brevity.).

The generalized intensity factors K on each crack edge are respectively obtained as follows:

(I) on inner crack edge, $x=l_1$ and $0\le y<l_2$:

$$K_x^{\mathrm{I}}=\lim_{x\to l_1}\sqrt{2(l_1-x)}\cdot\sigma_{1zz}=\frac{h_0}{\pi^2}\frac{\sqrt{2}}{\sqrt{l_3-l_1}}\sum_{n=0}^{\infty}\sum_{m=0}^{\infty}(-1)^{m+1}c_{mn}H_{1mn}(y) \tag{24}$$

$$K_{Dx}^{\mathrm{I}}=\lim_{x\to l_1}\sqrt{2(l_1-x)}\cdot D_{1z}=\frac{h_{70}}{\pi^2}\frac{\sqrt{2}}{\sqrt{l_3-l_1}}\sum_{n=0}^{\infty}\sum_{m=0}^{\infty}(-1)^{m+1}c_{mn}H_{1mn}(y) \tag{25}$$

$$K_{Bx}^{\mathrm{I}}=\lim_{x\to l_1}\sqrt{2(l_1-x)}\cdot B_{1z}=\frac{h_{80}}{\pi^2}\frac{\sqrt{2}}{\sqrt{l_3-l_1}}\sum_{n=0}^{\infty}\sum_{m=0}^{\infty}(-1)^{m+1}c_{mn}H_{1mn}(y) \tag{26}$$

(II) on outer crack edge, $x=l_3$ and $0\le y<l_2$:

$$K_x^{\mathrm{E}}=\lim_{x\to l_3}\sqrt{2(x-l_3)}\cdot\sigma_{1zz}=-\frac{h_0}{\pi^2}\frac{\sqrt{2}}{\sqrt{l_3-l_1}}\sum_{n=0}^{\infty}\sum_{m=0}^{\infty}c_{mn}H_{1mn}(y) \tag{27}$$

$$K_{Dx}^{\mathrm{E}}=\lim_{x\to l_3}\sqrt{2(x-l_3)}\cdot D_{1z}=-\frac{h_{70}}{\pi^2}\frac{\sqrt{2}}{\sqrt{l_3-l_1}}\sum_{n=0}^{\infty}\sum_{m=0}^{\infty}c_{mn}H_{1mn}(y) \tag{28}$$

$$K_{Bx}^{\mathrm{E}}=\lim_{x\to l_3}\sqrt{2(x-l_3)}\cdot B_{1z}=-\frac{h_{80}}{\pi^2}\frac{\sqrt{2}}{\sqrt{l_3-l_1}}\sum_{n=0}^{\infty}\sum_{m=0}^{\infty}c_{mn}H_{1mn}(y) \tag{29}$$

(III) on upper crack edge, $y=l_2$ and $l_1<x<l_3$:

$$K_y=\lim_{y\to l_2}\sqrt{2(y-l_2)}\cdot\sigma_{2zz}=\frac{2h_0}{\pi^2\sqrt{l_2}}\sum_{n=0}^{\infty}\sum_{m=0}^{\infty}c_{mn}R_{2m}(x)Q_{mn} \tag{30}$$

$$K_{Dy}=\lim_{y\to l_2}\sqrt{2(y-l_2)}\cdot D_{2z}=\frac{2h_{70}}{\pi^2\sqrt{l_2}}\sum_{n=0}^{\infty}\sum_{m=0}^{\infty}c_{mn}R_{2m}(x)Q_{mn} \tag{31}$$

$$K_{By}=\lim_{y\to l_2}\sqrt{2(y-l_2)}\cdot B_{2z}=\frac{2h_{80}}{\pi^2\sqrt{l_2}}\sum_{n=0}^{\infty}\sum_{m=0}^{\infty}c_{mn}R_{2m}(x)Q_{mn} \tag{32}$$

where $Q_{mn} = -2\pi \dfrac{\Gamma(m+1+\frac{1}{2})}{m!} \dfrac{\Gamma(2n+1+\frac{1}{2})}{(2n)!}$.

6 NUMERICAL RESULTS AND DISCUSSION

Now, the analytical solution for generalized intensity factors have been derived strictly in forms of infinite polynomials, but to demonstrate the response law of cracks to kinds of factors such as loading frequency, numerical results are calculated and depicted for the generalized intensity factors. Considering the commonly used magneto-electro-elastic materials, the material constants of $BaTiO_3/CoFe_2O_4$ are adopted in all computations as shown in Table 1 to Table 3. According to the previous work[15], to achieve the available numerical solutions through the Schmidt method, only the first several terms in the infinite series should be taken into calculation. Here, the top ten terms are taken in computation, and the numerical results of the generalized intensity factors are graphically shown from Fig. 2 to Fig. 5 to indicate some significant response laws different from the static problem.

c_{11} (N/m^2)	c_{12} (N/m^2)	c_{13} (N/m^2)	c_{33} (N/m^2)	c_{44} (N/m^2)	ρ (kg/m^3)
22.6×10^{10}	12.5×10^{10}	12.4×10^{10}	21.6×10^{10}	4.4×10^{10}	5500.0

Table 1: Elastic stiffness constants and mass density of $BaTiO_3$-$CoFe_2O_4$

e_{31} (C/m^2)	e_{33} (C/m^2)	e_{15} (C/m^2)	f_{31} (N/Am)	f_{33} (N/Am)	f_{15} (N/Am)
–2.2	9.3	5.8	290.2	350.0	275.0

Table 2: Piezoelectric constants and piezomagnetic constants of $BaTiO_3$-$CoFe_2O_4$

ε_{11} (C^2/Nm^2)	ε_{33} (C^2/Nm^2)	μ_{11} (Ns^2/C^2)	μ_{33} (Ns^2/C^2)	g_{11} (Ns/VC)	g_{33} (Ns/VC)
56.4×10^{-10}	63.5×10^{-10}	297.5×10^{-6}	83.5×10^{-6}	4.0×10^{-9}	4.7×10^{-9}

Table 3: Dielectric constants, magnetic permeablities and electromagnetic constants of BaTiO3-CoFe2O4

(I) According to Eqs.(24)-(32), the stress intensity factors, the electric intensity factors and the magnetic flux intensity factors possess of the same changing rule and only different in magnitudes coming from h_0, h_{70} and h_{80}, which had been discussed in references [9, 17]. So during the following discussion, the electric displacement intensity factors and the magnetic flux intensity factors would not be elaborated particularly for the simplicity of

the article, except the generalized intensity factors show a different variation.

(II) Maintain the circular frequency ω satisfying $\omega l_2 / c_z = 0.8$ and $\omega l_2 / c_z = 1.2$, respectively, the stress intensity factors at the midpoints on the inner crack edge, the outer crack edge and the upper crack edge are depicted versus the inter space between two rectangular cracks as shown in Fig.2 and Fig.3. All stress intensity factors vibrate with the increasing of l_1, with the vibration amplitudes gradually tending to zero. Different from statistic problems that the stress intensity factor on the inner crack edges is always larger than ones on the outer crack edges, as shown in Fig.2(a) and Fig.3(a), the stress intensity factors at inner and outer crack edge alternately occupy the dominant position, which makes it more difficult to predicting crack converging. When $\omega l_2 / c_z = 0.8$, the cracks are more inclined to converging for $l_1 / l_2 < 0.5$. When $\omega l_2 / c_z = 1.2$, the cracks will expand outward separately for $l_1 / l_2 < 0.5$. But for $l_1 / l_2 \geq 0.5$, even though the stress intensity factor on one edge is slightly larger than that on the other edge, it is hard to say whether cracks join together or expand separately. Additionally, the stress intensity factors at the midpoint on the upper edge are smaller than that on the inner and outer edges in these two cases.

(III) Fig.4 depicts the trend of K^* at midpoint on each crack edge versus the dimensionless circular frequency $\omega_0 = \omega l_1 / c_z$. Within the researched load frequency range, when the frequency is not large $\omega_0 < 1.0$, the two cracks are capable of converging. However, with larger ω_0, the main behavior of two coplanar cracks is enlarging separately. Note that, as shown in Fig.4, the most dangerous load frequency prompting cracks to converge locates at $\omega_0 \approx 0.7$. Additionally, in the case of dangerous frequency, the midpoint of crack edge is not the location easy to crack according to the stress intensity factors curve as shown in Fig.5. the whole crack edges should be given adequate attention in the dynamic fracture analysis.

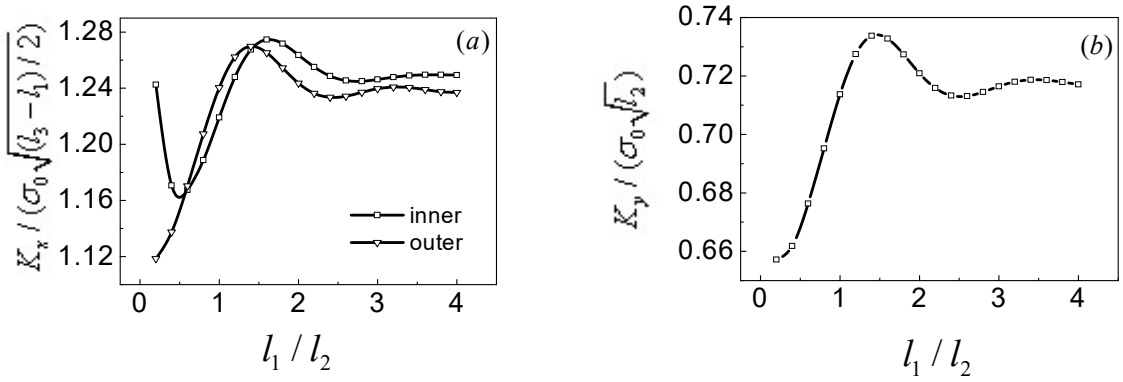

Fig.2: The stress intensity factors versus l_1 / l_2 for $l_2 = 1.0$, $l_3 - l_1 = 1.0$, $\omega l_2 / c_z = 0.8$, $D_0 / \varepsilon_0 = 1.0 \times 10^8$ and $B_0 / \mu_0 = 1.0 \times 10^5$.

(a) The stress intensity factors at the middle point of inner and outer crack edges

(b) The stress intensity factors at the middle point of upper crack edge

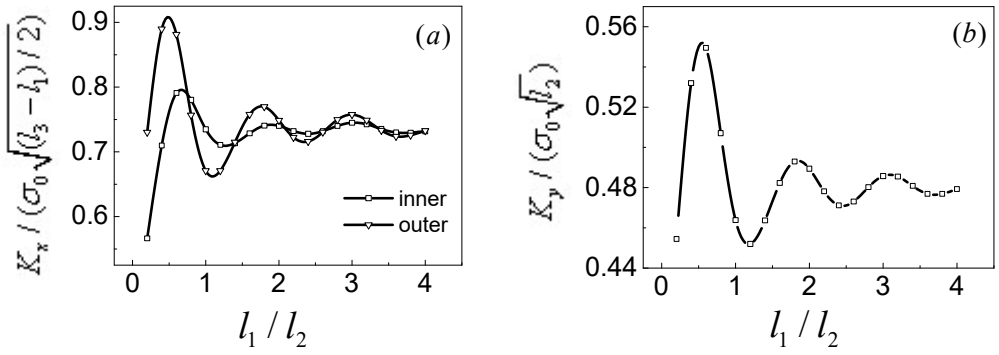

Fig.3: The stress intensity factors versus l_1 / l_2 for $l_2 = 1.0$, $l_3 - l_1 = 1.0$, $\omega l_2 / c_z = 1.2$, $D_0 / \varepsilon_0 = 1.0 \times 10^8$ and $B_0 / \mu_0 = 1.0 \times 10^5$.

(a) The stress intensity factors at middle points of inner and outer crack edges

(b) The stress intensity factors at the middle point of upper crack edge

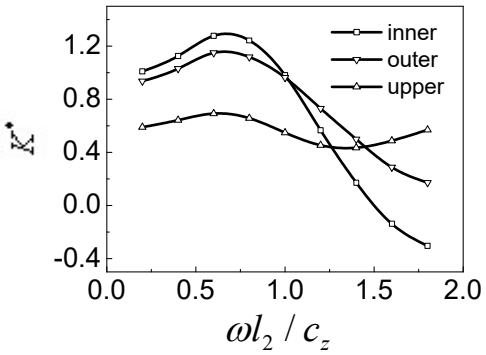

Fig.4: The stress intensity factors at middle point of inner, outer and upper crack edge versus $\omega l_2 / c_z$ for $l_1 = 0.2$, $l_2 = 1.0$, $l_3 = 1.2$, $D_0 / \varepsilon_0 = 1.0 \times 10^8$ and $B_0 / \mu_0 = 1.0 \times 10^5$.

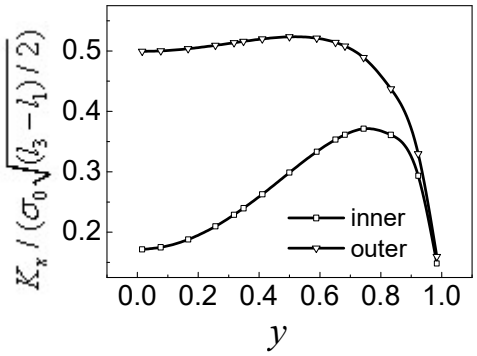

Fig.5: The stress intensity factors on inner and outer crack edges versus y for $l_1 = 0.2$, $l_2 = 1.0$, $l_3 = 1.2$, $\omega l_2 / c_z = 1.4$, $D_0 / \varepsilon_0 = 1.0 \times 10^8$ and $B_0 / \mu_0 = 1.0 \times 10^5$.

7 CONCLUSIONS

Coupling fracture of coplanar two rectangular cracks was addressed considering piezoelectric effect, piezomagnetic effect and magneto-electric effect of materials and the load frequency. limited-permeable crack model was introduced to emulating the reality and using generalized Almansi' theorem and Fourier Transform, the analytical solution of whole generalized fields and generalized intensity factors were deduced strictly. In order to demonstrate intuitively the affection of geometry of cracks and load frequency on the initiation behavior of cracks, numerical computation was depicted with the help of Schmidt method which permitted higher accuracy with less computation. Some important factors affecting fracture behavior were pointed out to advance the material health monitory.

ACKNOWLEDGMENTS

This work was supported by the National Natural Science Foundation of China (11202050) and Jiangsu Natural Science Foundation of China(BK2012318).

REFERENCE

[1] J. Vansuchtelen, Product properties-new application of composite-materials. *Philips Research Reports*, **27**, 28-37, 1972

[2] J.K. Du, Y.P. Shen, B. Gao, Scattering of anti-plane shear waves by a single crack in an unbounded transversely isotropic electro-magneto-elastic medium. *Appl Math Mech-engl*, **25**, 1344-1353, 2004.

[3] G.C. Sih, Z.F. Song, Magnetic and electric poling effects associated with crack growth in BaTiO3-CoFe2O4 composite. *Theor Appl Fract Mech*, **39**, 209-227, 2003.

[4] X.C. Zhong, X.F. Li, A finite length crack propagating along the interface of two dissimilar magnetoelectroelastic materials. *Int J Eng Sci*, **44**, 1394-1407, 2006.

[5] X.C. Zhong, Analysis of a dielectric crack in a magnetoelectroelastic layer. *Int J Solids Struct*, **46**, 4221-4230, 2009.

[6] W.J. Feng, Y. Xue, Z.Z. Zou, Crack growth of an interface crack between two dissimilar magneto-electro-elastic materials under anti-plane mechanical and in-plane electric magnetic impact. *Theor Appl Fract Mech*, **43**, 376-394, 2005.

[7] W.J. Feng, Y.S. Li, Z.H. Xu, Transient response of an interfacial crack between dissimilar magnetoelectroelastic layers under magnetoelectromechanical impact loadings: Mode-I problem. *Int J Solids Struct*, **46**, 3346-3356, 2009.

[8] T.H. Hao, Z.Y. Shen, A New Electric Boundary-Condition of Electric Fracture-Mechanics and Its Applications. *Eng Fract Mech*, **47**, 793-802, 1994.

[9] Z.G. Zhou, P.W. Zhang, L.Z. Wu, Solutions to a limited-permeable crack or two limited-permeable collinear cracks in piezoelectric/piezomagnetic materials. *Arch Appl Mech*, **77**, 861-882, 2007.

[10] X.C. Zhong, X.F. Li, Magnetoelectroelastic analysis for an opening crack in a piezoelectromagnetic solid. *Eur J Mech A-solid*, **26**, 405-417, 2007.

[11] Z.G. Zhou, Z.T. Chen, Basic solution of a Mode-I limited-permeable crack in functionally graded piezoelectric/piezomagnetic materials. *Int J Solids Struct*, **45**, 2265-2296, 2008.

[12] X.F. Li, K.Y. Lee, Crack growth in a piezoelectric material with a Griffith crack perpendicular to the poling axis. *Philos Mag*, **84**, 1789-1820, 2004.

[13] W.Q. Chen, K.Y. Lee, H. Ding, General solution for transversely isotropic magneto-electro-thermo-elasticity and the potential theory method. *Int J Eng Sci*, **42**, 1361-1379, 2004.

[14] P.M. Morse, H. Feshbach, *Methods of Theoretical Physics*. McGraw-Hill, 1958.

[15] S. Itou, 3-Dimensional wave-propagation in a cracked elastic solid. *J Appl Mech-t Asme*, **45**, 807-811, 1978.

[16] P.W. Zhang, Z.G. Zhou, L.Z. Wu, Coupled field state around three parallel non-symmetric cracks in a piezoelectric/piezomagnetic material plane. *Arch Appl Mech*, **79**, 965-979, 2009.

[17] P.W. Zhang, Z.G. Zhou, B. Wang, Dynamic behavior of two collinear interface cracks between two dissimilar functionally graded piezoelectric/piezomagnetic material strips. *Appl Math Mech-engl*, **28**, 615-625, 2007.